AIAA JOURNAL
Vol. 35, No. 11, November 1997

Two-Component Planar Doppler Velocimetry in High Speed Flows

Pamela S. Clancy* and Mo Samimy†
The Ohio State University, Columbus, Ohio 43210

A planar Doppler velocimetry technique was developed and used to measure two components of instantaneous velocity in an ideally expanded, Mach 2, freejet. The technique utilizes a molecular filter as a frequency discriminator and uses two cameras to resolve two components of velocity on a plane that is illuminated by a laser sheet. Careful formation of the laser sheet, proper calibration of the splitter/recombiner imaging system, and precise image registration were found to be critical steps in the technique. The velocity measurements obtained with this technique were compared with reference laser Doppler velocimetry measurements taken in the same flowfield. The mean velocity results were in very good agreement with the reference measurements, and the turbulence results captured the correct trend but were higher than the reference results. A detailed error analysis describes the error sources inherent in the planar Doppler velocimetry technique. For the current two-component planar Doppler velocimetry system, the estimated uncertainty for the *x* and *y* components of velocity were ±5 and ±3.5% of the jet centerline velocity, respectively. The errors in the *x* component of velocity were within the estimated uncertainty. The errors in the *y* component of velocity exceeded the estimated uncertainty. Possible causes for this difference are discussed.

I. Introduction

CURRENTLY, there are a number of planar optical velocimetry techniques that are being advanced. One of the more powerful techniques is the planar Doppler velocimetry (PDV) technique. The PDV technique, by incorporating a molecular filter to resolve the Doppler shift of particles scattering laser light in a flowfield, is capable of making velocity measurements in a two-dimensional measurement volume. Furthermore, three components of instantaneous velocity can be resolved when using a high-power, short-duration, pulsed laser and three Doppler shift measuring systems.

Researchers have been using molecular filters to resolve Doppler shifted signals in various capacities for a number of years. Different information can be obtained based on the type of scattering involved. If the scattering is classified as Mie or Rayleigh/Mie scattering, only the Doppler shift can be measured. If the scattering is classified as Rayleigh scattering, then density, temperature, and pressure information, in addition to the Doppler shift, can be measured.

Some of the techniques which use filters include, filtered Rayleigh scattering (FRS), which refers to the use of a molecular filter to remove unwanted background signals in flow visualizations[1] and to remove Rayleigh scattering signals to detect much lower intensity Raman scattering signals.[2] FRS also refers to the technique of tuning the laser frequency and then using the deconvolution of the Rayleigh scattered intensity profile from the filter transmission profile to extract the average flow velocity, temperature, and pressure.[3] The molecular filter can also be used with Rayleigh scattering and an anamorphic optical system to measure instantaneous velocity, temperature, and pressure.[4,5] Furthermore, frequency modulated-FRS has been investigated as a possible real-time, in-flight, velocity sensor.[6]

Combining Rayleigh/Mie or Mie scattering with a molecular filter is the basis of PDV.[7–13] A technique very similar to PDV, referred to as Doppler global velocimetry (DGV), has been developed in parallel and is used by various researchers.[14–16] The bases of PDV and DGV are fundamentally the same.

The procedure and subtle details of the PDV technique continue to be refined and explored. Elliott et al.[7] established a PDV technique referring to it as filtered planar velocimetry. The technique was successfully employed to measure a single velocity component in compressible mixing layers. Two cameras were used in the experiments; one camera to obtain the filtered image and the second camera to obtain the reference image. Arnette et al.[8] furthered the PDV technique by establishing a two-component PDV system. The system was used to measure two components of velocity in supersonic boundary layers. They used three cameras to obtain two components of velocity. Two cameras were used to obtain the filtered image from two different viewing angles and the third camera served as the reference camera for both of the filtered images. Smith et al.[11] significantly advanced the procedure of a one-component PDV system and measured the flow velocity of perfectly expanded and overexpanded supersonic jets. They employed a splitter/recombiner system such that only one camera was used to obtain both the filtered and unfiltered images. McKenzie[9,10] documented the measurement capabilities of PDV with various light levels and camera qualities and also investigated the minimum velocity resolution obtainable with a one-component PDV system, applied to a low-speed flow, using a pulsed laser. He also presented a detailed description of the error sources associated with camera related noise and highlighted the benefits of binning the camera pixels. Clancy et al.[12] advanced the PDV technique by incorporating the splitter/recombiner system and a frequency monitoring system, suggested by various researchers,[7,9,11,17] into a two-component PDV system. Additional results by Clancy and Samimy[13] identified the need for improved PDV procedures to account for issues concerning the laser sheet formation, image registration, and proper calibration of the split imaging system.

This work highlights the fundamental issues behind the PDV technique and establishes a set of PDV procedures that results in accurate velocity measurements. The technique was used to obtain planar measurements of two components of instantaneous velocities in a Mach 2, axisymmetric, ideally expanded, freejet. The PDV measurements are compared with laser Doppler velocimetry (LDV) measurements. In addition, a detailed discussion of the error sources involved in the PDV experiments is provided along with an overall uncertainty estimate.

II. Basics of PDV

PDV is a nonintrusive, optical diagnostic technique used to measure velocity on a given plane in a flow. It employs a molecular filter as a frequency discriminator to measure the Doppler shifted frequency of light, from a narrow linewidth laser, scattered by particles

Received Jan. 30, 1997; revision received May 23, 1997; accepted for publication July 31, 1997.

*Graduate Researcher, Department of Mechanical Engineering. Student Member AIAA.

†Professor and Associate Chair, Department of Mechanical Engineering. Associate Fellow AIAA.

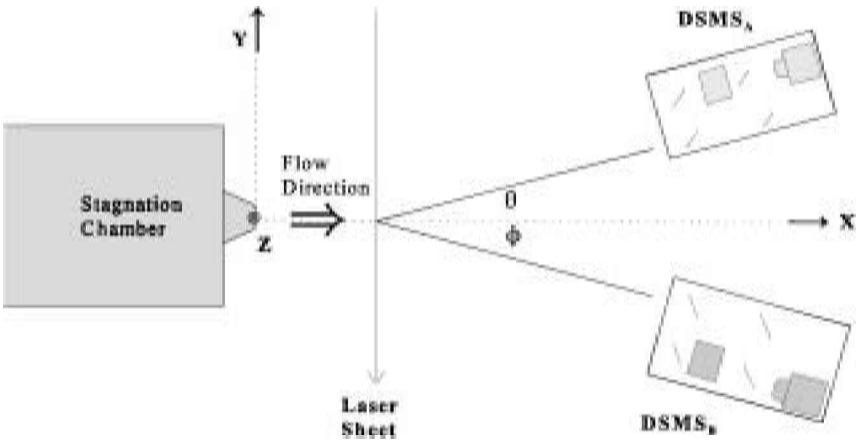

Fig. 1 Schematic of a two-component PDV system with the coordinate system defined; jet axis is aligned with x axis, the laser is propagating in the negative y direction, and the DSMSs are in the x–y plane.

in the flowfield. The scattering is produced as seeded particles and/or naturally occurring particles in the flowfield pass through the laser sheet. The scattered light will be Doppler shifted in frequency from the laser frequency according to[18]

$$\Delta f_d = \frac{(\boldsymbol{s} - \boldsymbol{o})}{\lambda} \cdot \boldsymbol{V} \tag{1}$$

where $\boldsymbol{o}$ is the unit vector pointing in the propagating direction of the laser light and $\boldsymbol{s}$ is the unit vector pointing in the direction of observation. Both vectors $\boldsymbol{o}$ and $\boldsymbol{s}$ are selected by the investigator. $\boldsymbol{V}$ is the particle velocity to be determined, and λ is the wavelength of the laser light.

The technique can be configured to measure one to three components of velocity. A schematic of a two-component system is shown in Fig. 1. The intersection of the light sheet with the flowfield defines the measurement volume. If a pulsed laser is used, with the pulse duration being small in comparison with the time scale of the flow, then the velocity measurements can be considered instantaneous. Therefore, when a high-energy pulsed laser is used, PDV can be used to obtain planar instantaneous velocities.

The power of PDV resides in the use of the molecular filter as a frequency discriminator to measure the Doppler shift for a planar interrogation region. Physically, the filter is a sealed glass cell containing a prescribed amount of molecular or atomic vapor. The amount and type of vapor used are dependent on the laser wavelength and the expected Doppler shift range. The partial pressure of the vapor contained in the cell, the cell length, and the cell temperature govern the transmission profile of the filter, which is a function of frequency.

In a PDV experiment, filtered and unfiltered images of the flowfield are collected with each Doppler shift measuring system (DSMS) (Fig. 1). The filtered image passes through the filter before being recorded, and the unfiltered image is directly recorded. The ratio of each point in the filtered image with the corresponding point in the unfiltered image is the transmission coefficient. Knowing the transmission profile of the filter, which is a function of frequency, and the transmission coefficient, obtained from the filtered and unfiltered images, the scattered frequency relative to the laser frequency is determined. This procedure is used to determine the Doppler shift of each point in the flowfield for each DSMS. Equation (1) is then used to resolve the instantaneous velocities.

The application of a two-component PDV system is presented, using refined data collection and processing procedures to measure the instantaneous velocity in a Mach 2, axisymmetric freejet. In the process, certain procedural steps were found to be critical in obtaining accurate PDV results. These steps include proper formation of the laser sheet, accurate calibration procedures, and subpixel image registration. Each of these steps will be discussed in detail, and the two-component results will be presented. The PDV velocity results are compared with LDV measurements of the same flowfield. In addition, a detailed error analysis is discussed.

III. Experimental Setup and Procedure

Setup

A PDV system was established and used to resolve two components of instantaneous velocity in a Mach 2, axisymmetric freejet. The cross-stream plane measurement volume, the intersection of the laser sheet with the jet flow, was located 6.3 jet diameters downstream of the 1.9-cm-diam jet exit. The x and y components of velocity (as defined in Fig. 1) were obtained. Two DSMSs were used to resolve the x and y components of velocity. As shown in Fig. 1, $\mathrm{DSMS_A}$ and $\mathrm{DSMS_B}$ were located in the x–y plane at a viewing angle of $\theta = +24.5$ deg and $\phi = -23.5$ deg, respectively, from the jet centerline. For this configuration, with the laser sheet propagating in the negative y direction, the Doppler shift equations for $\mathrm{DSMS_A}$ and $\mathrm{DSMS_B}$, respectively, were

$$\begin{aligned} \lambda \Delta f_{d_A} &= V_x \cos(\theta) + V_y[1 + \sin(\theta)] \\ \lambda \Delta f_{d_B} &= V_x \cos(\phi) + V_y[1 + \sin(\phi)] \end{aligned} \tag{2}$$

The flow was unheated, and the jet was operated in the ideally expanded regime. The Reynolds number based on the jet exit diameter was 2.1×10^6. The laser was an injection seeded Nd:YAG Quanta Ray laser operating at a 532-nm wavelength with 510 mJ/pulse. The laser had a 9-ns pulse duration, 10-Hz repetition rate, and an approximate linewidth of 100 MHz. The images were collected on Princeton Instruments, Inc., cooled, intensified, 14-bit, charge-coupled device (CCD) cameras. A Tamaron SPF2BB camera lens, with an indicated f number of approximately 6.8, was used with each camera. All images were collected by operating the camera in a bin by 2 mode. Because the camera array was 576×384 pixels, operating the camera in a bin by 2 mode resulted in images consisting of 288×192 superpixels. For simplicity, in the sequel these superpixels are referred to as pixels. Each pixel in the raw image corresponded to an object size of 750-μm square. The signal level was strong, and the velocity was calculated for points where the signal to background noise ratio was better than 10.

The experiments were conducted at the Aeronautical and Astronautical Research Laboratory of Ohio State University. Dry and compressed air was stored in two storage tanks with a total capacity of 42.5 $\mathrm{m^3}$ at 17 MPa. The jet stagnation pressure and stagnation temperature were monitored during the experiments. Data collection commenced when the stagnation temperature had settled. The stagnation pressure was maintained within 2% of the desired pressure.

The seed particles consisted of naturally generated ice clusters and seeded acetone. The ice clusters formed when warm moist ambient air mixed with the cold jet flow. Because the ice clusters only marked regions of the mixing layer, acetone from a pressurized tank was seeded into the stagnation chamber to mark the jet core. The amount of acetone seeding was estimated, by measuring the drop in acetone level in the seed tank with time, to be approximately 0.4% of the air-flow by weight. The diameter of the ice clusters and acetone clusters was expected to be on the order of 50 nm. This

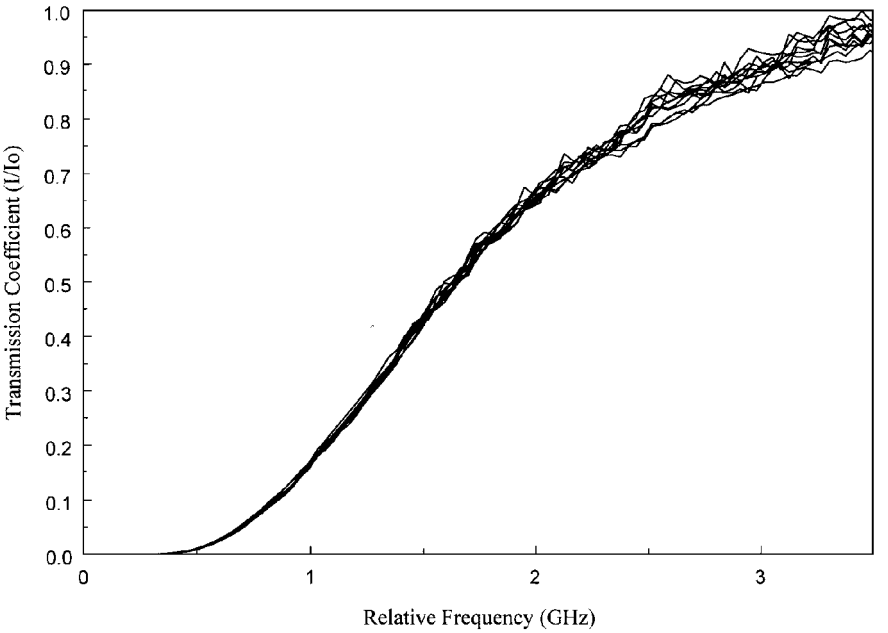

Fig. 2 Overlay of transmission profiles for various heights of a laser sheet formed from more than 80% of the centermost portion of the laser beam.

was deduced by Ref. 19 because the scattering of the 532-nm wavelength of a Nd:YAG laser light from such particles fell in between the Rayleigh and Mie scattering regimes. Furthermore, based on previously reported results,[20] these particles were expected to follow the flow.

Molecular Filter

A molecular filter was used to measure the Doppler shifted frequency of the scattered light. The filter had a transmission profile that was a function of frequency. The profile was governed by the dimensions of the filter and the thermodynamic properties of the vapor contained in the filter. Each filter was 10 cm in length and 10 cm in diameter. Details of how to prepare a filter can be found in Ref. 7. The filter transmission profile was determined experimentally. The amount of iodine and nitrogen contained in the filter was determined by trial and error until the desired transmission profile was obtained for the expected flow Doppler shifts. Each filter contained 4.28 torr of I_2 and 41 torr of N_2. Each filter was wrapped in two strips of Omega Omegalux heat tape and insulation. For both filters, the filter temperature, controlled by an Ohmite variable transformer, was held at approximately 174°C. The absorption line of iodine at 18,788.4 cm^{-1} was used in these experiments.

A frequency doubled, injection seeded, 10-Hz, Nd:YAG laser was used. The frequency was changed by changing the seeder frequency control voltage. The filter transmission profile was determined by incrementing the seeder frequency control voltage and obtaining filtered and unfiltered images of scattering from a stationary source. Thus for each frequency, the filter transmission was determined. The conversion factor from seeder frequency control voltage to laser frequency was obtained by comparing an experimentally determined transmission profile with a theoretical transmission profile.[9,13,17]

In the PDV experiment, the filter transmission profile was experimentally determined at the beginning and end of the experiment. In addition, the frequency of the laser was monitored as it was incremented to the desired frequency for the velocity measurements.

Laser Sheet

The velocity measurements were made in a plane defined by the intersection of the laser sheet and the jet flow. The laser sheet was formed by directing the beam through two cylindrical lenses, a spherical lens and a plano-convex lens. The collimated laser sheet thickness was determined, by taking a burn pattern, to be less than 400 μm. The orientation of the laser sheet was specified with respect to the coordinate system defined in Fig. 1. A major concern in setting up the laser sheet was the consistency of the frequency across the laser sheet. References 3 and 17 noted a variation of frequency within their laser beam of about 100 MHz. A variation of the frequency content across the current laser sheet was also noticed. However, with careful arrangement, as will be discussed, the laser sheet was formed such that the laser frequency content was consistent throughout the measurement volume. The filter transmission profile was based on the scattering from a stationary source. The laser sheet passing through a glass container filled with water and trace amounts of powdered milk provided the stationary scattering. Using this configuration, the filter transmission profile was calculated for various heights across the laser sheet. The resulting transmission profiles for various heights were compared for different laser sheet setups. Figure 2 shows the calculated filter transmission profiles for various vertical positions for a laser sheet formed from more than 80% of the centermost portion of the laser beam. As can be seen in Fig. 2, there was a distinct variation in the filter transmission profile across the laser sheet. The variations were believed to be due to variations in frequency content of the laser beam. However, Fig. 3, obtained with a laser sheet formed from less than 60% of the centermost part of the laser beam, shows negligible variation of the filter transmission profile. The variation of the filter transmission profile across the laser sheet for the velocity data herein was less than 4 MHz. In general, forming the laser sheet from the centermost portion of the laser beam produced a laser sheet having a more consistent frequency content.

Splitter/Recombiner System

As was discussed earlier, a set of images, consisting of filtered and unfiltered images, was required for each viewing direction. Previous investigators used separate cameras for the filtered and unfiltered images.[7,8] The PDV setup herein used a splitter/recombiner imaging system.[9–13] In this system, the filtered and unfiltered images were collected side-by-side on one camera. In this configuration, one camera was required for each component of velocity. The requirement of three cameras to measure three components of velocity was a significant reduction from the six cameras previously required. Figure 4 is a schematic of a splitter/recombiner system. The beam splitter split the scattered image. The unfiltered image was directed by mirrors and was collected by one part of the camera. The filtered image was directed such that the light passed through the filter before being collected by a different part of the same camera. In setting up the splitter/recombiner imaging system, it was important to visually check that both images were in focus and did not overlap.

Accurately registering the filtered and unfiltered images was the most important step in the PDV procedure. As will be subsequently demonstrated, subpixel accuracy in the alignment was required. To

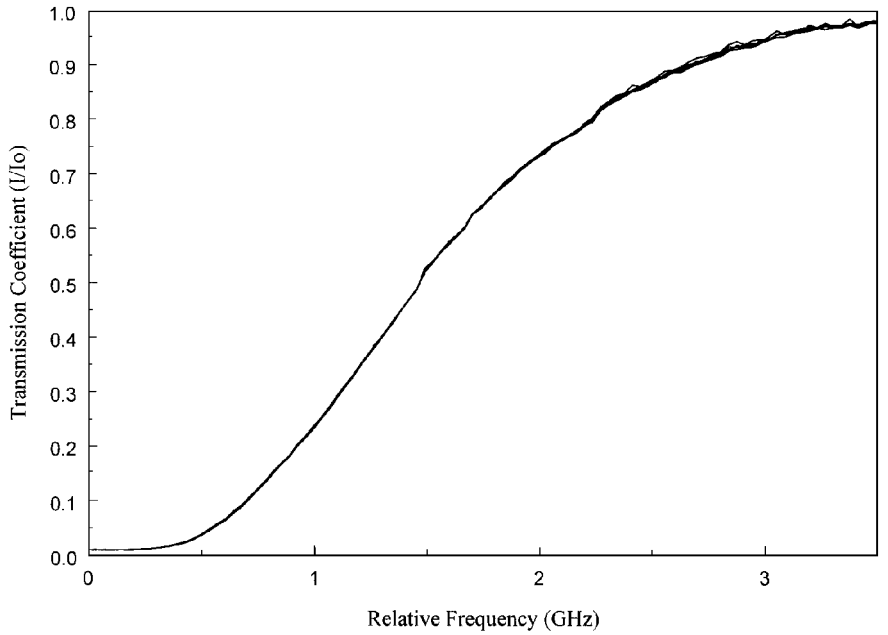

Fig. 3 Overlay of transmission profiles for various heights of a laser sheet formed from less than 60% of the centermost portion of the laser beam.

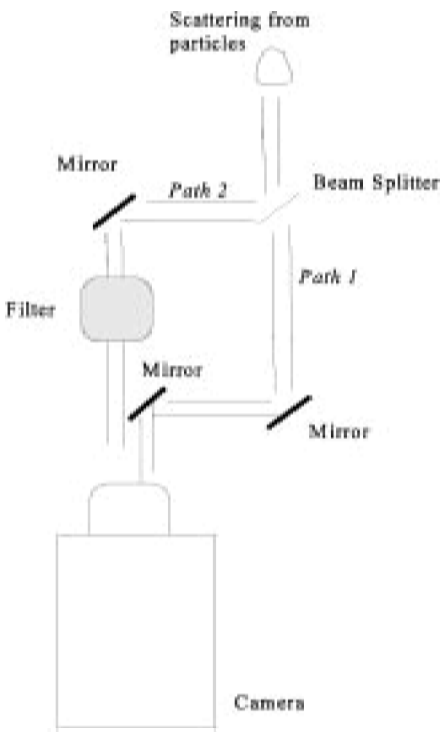

Fig. 4 Schematic of a split imaging system (splitter/recombiner) system; path 1 is directly focused onto the camera, and path 2 passes through the filter before being focused onto the camera.

obtain subpixel accuracy, a grid consisting of white dots on a black background was taken in normal room light and was used as a reference image. The centroid of each point was determined for the filtered and unfiltered regions. The corresponding vertical and horizontal shifts needed to align the filtered and unfiltered regions were calculated for the grid points. The shifts for all nongrid points were calculated by using a two-dimensional linear interpolation scheme. First, the filtered and unfiltered images were aligned and the Doppler shifts for each DSMS were determined. Then, to resolve the velocity components, the same basic process was used to align the velocity images from $DSMS_A$ with $DSMS_B$. Although this process resulted in accurate velocity measurements, the technique can be further improved.

Flatfield Images

Another key step in the PDV procedure was the proper calibration of the splitter/recombiner system. Because of the nature of the split imaging system, calibration was required to account for optical variations across each image and for the polarization dependent quality of the beam splitters. A flatfield image was required to normalize the images used in experimentally calibrating the filter, i.e., the filter transmission images, and for the images used to calculate the velocity, i.e., the velocity images. Because the filter is an optical component of the splitter/recombiner system, it was in place when the calibration images that constituted the flatfield images were taken. For example, the velocity flatfield image was the average of a 100 velocity calibration images. The velocity calibration images were taken under the same conditions as the velocity images except the laser frequency was set to full filter transmission of the filter. The laser frequency was set to full filter transmission since the filter was in place in the splitter/recombiner system when the calibration images were obtained and the calibration images should not be sensitive to flow velocity. An analogous procedure was performed to calculate the filter transmission flatfield image. The flatfield images were used to normalize the filter transmission and velocity images for optical distortions, for variations in the images due to the polarization-dependent characteristic of the beam splitters, and for variations of camera gain.

Laser Frequency Variations with Time

Finally, the laser frequency fluctuates and drifts. The pulse-to-pulse variations in the laser frequency are random fluctuations in time about a mean and that mean may slowly drift in time. Because the measured Doppler shift is relative to the laser frequency, any variation of laser frequency corresponds to an error in the determined Doppler shift and resulting velocity calculations. A system to monitor the laser frequency has been developed and implemented.[12] However, preliminary data indicated the need for improved PDV procedures.[12] Because the goal of the present experiments was to establish a set of refined PDV procedures, the frequency monitoring system was not used. The laser frequency fluctuations may cause errors in the instantaneous velocity and the turbulence intensity. However, because the fluctuations vary about a mean, the fluctuations are, for the most part, averaged out of the mean velocity calculations. Thus, the mean velocity measurements are minimally affected by the frequency fluctuations. The slower drift of the laser frequency, if present, affects the magnitude of the velocity measurements. Because the mean velocity results in the present experiments were quite accurate, as will be presented and discussed next, the drift of the laser for this data set was assumed to have been negligible.

IV. Experimental Results

A set of 200 velocity images was obtained at the desired laser frequency, and a set of 200 velocity calibration images was obtained at a laser frequency corresponding to full transmission of the molecular filters. Figure 5 displays an instantaneous velocity image set for $DSMS_A$ and $DSMS_B$. Only images that had a minimal number of saturated pixels were used in the velocity and flatfield calculations. Unfortunately, this dropped the velocity image set from 200 to 71. A very important point is that the average velocity, at any given point, was calculated by taking the average of the instantaneous velocities over these 71 images. For the magnitude and range of the Doppler shifts realized in supersonic flows the optically thick filters utilized here are pressure broadened. As a result, the filter transmission profile is not linear over the entire range used, and averaging the images and then calculating the velocity will result in erroneous velocity measurements.[11] Thus, for supersonic flows, Nd:YAG lasers are ideal in that they can provide enough energy for instantaneous planar velocity measurements.

Figure 6 displays the velocity maps for the resolved x and y components of velocity. The first column is the x component of velocity and the second column is the y component of velocity. The top row shows the average velocities, and the second and third rows show the instantaneous velocities for two random instants in time. For each map, the brightness is directly proportional to velocity and is scaled such that black corresponds to the slowest velocities and white corresponds to the fastest velocities. The size of each image corresponds to 23 mm in height and 36 mm in width. Figure 6 displays the instantaneous and planar capabilities of PDV. The coarse nature of the instantaneous velocity maps was due to image noise possibly caused by speckle. References 10 and 11 reported the occurrence of speckle in their PDV images. Speckle is produced when coherent light is scattered by a medium that introduces random optical path variations comparable to the optical wavelength.[21] The noise to signal ratio in the present PDV images was less than 0.15. The image noise did not have a noticeable effect on the mean velocities but was found to have a significant effect on the turbulence intensities. This image noise is discussed further in the error analysis section.

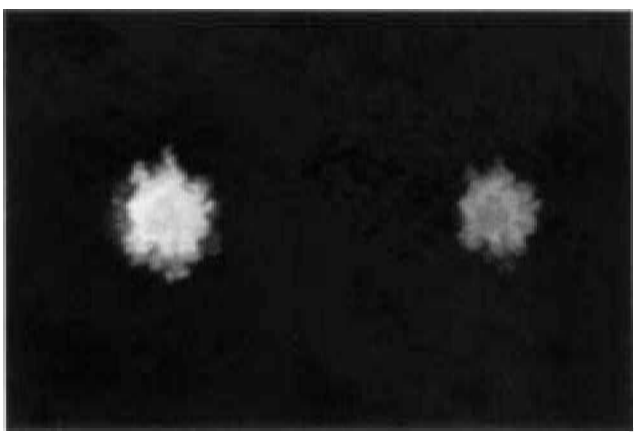

$DSMS_A$

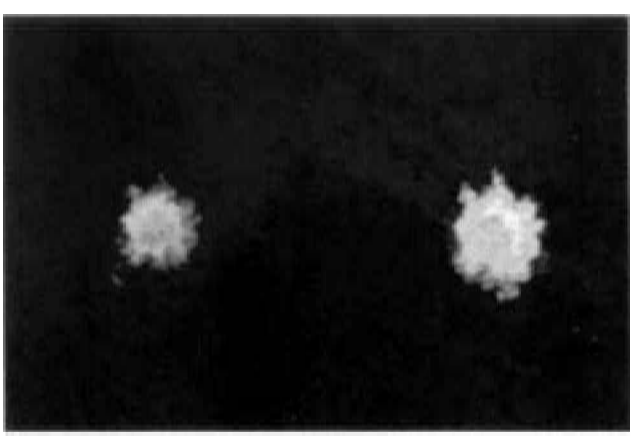

$DSMS_B$

Fig. 5 Example of an instantaneous image set consisting of a velocity image from each DSM.

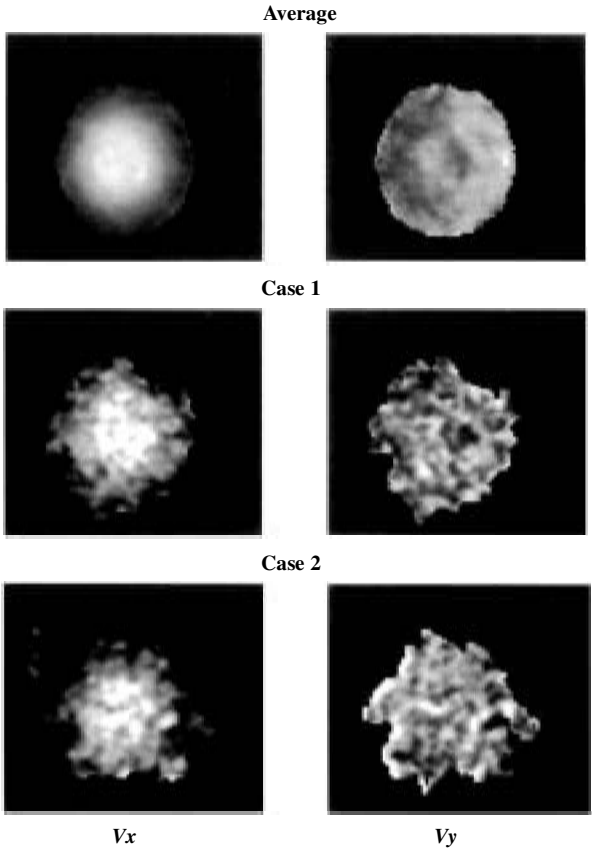

Fig. 6 Average and instantaneous two-component PDV results; for each image, the brightness is directly proportional to velocity and is scaled such that black corresponds to slower velocities and white corresponds to faster velocities.

Two postprocessing steps were used to reduce the effect of the noise on the turbulence intensities. The first step involved passing the raw images through a low-pass filter. The low-pass filtered intensity for the i, j pixel ($LPI_{i,j}$) was computed using the following equation with I denoting the original intensity:

$$\begin{aligned} LPI_{i,j} &= 0.0625 \times I_{i-1,j-1} + 0.125 \times I_{i-1,j} \\ &\quad + 0.0625 \times I_{i-1,j+1} + 0.125 \times I_{i,j-1} + 0.25 \times I_{i,j} \\ &\quad + 0.125 \times I_{i,j+1} + 0.0625 \times I_{i+1,j-1} \\ &\quad + 0.125 \times I_{i+1,j} + 0.0625 \times I_{i+1,j+1} \end{aligned} \tag{3}$$

Reference 22 discusses in detail methods, such as low-pass filtering, used to reduce image noise. Reference 11 also used low-pass filtering to decrease the effect of speckle in PDV images. The drawback of passing the images through a low-pass filter was the reduction in the spatial resolution. The second step used in an attempt to reduce the effect of the image noise is discussed later in relation to the turbulence intensities.

To check the accuracy of the PDV velocity results, a set of LDV velocity measurements was obtained. Because LDV is a well-established velocimetry technique, the LDV data were used as a reference for the PDV data. The data were obtained with a TSI, two-component, fiber-optic-based system consisting of a Colorburst, a fiber-optic probe, receiving optics, and an IFA-750 burst correlator. The green and blue beams, from a Spectra Physics 2020 argon ion laser, were shifted by 40 MHz to measure negative velocities and reduce fringe bias.[12] Because LDV is a pointwise measurement technique, average and rms measurements of the x and z component of velocity were only made along the vertical centerline of the jet, at a location of 6 jet diameters downstream of the jet exit. Because the jet is axisymmetric, the LDV data are treated as the x and y component of velocity along the horizontal centerline of the jet for comparing the LDV results with the PDV results.

Figure 7 compares the average PDV data with the average LDV data. All of the velocity measurements have been normalized by the jet centerline velocity V_c. Figure 7a displays the x and y components of velocity along the vertical centerline. The y component of velocity for the vertical centerline should be approximately zero. The PDV data agree extremely well with the LDV data for the x component of velocity, and the y component of velocity is approximately zero. Figure 7b displays the x and y components of velocity along the horizontal centerline of the jet. Again, the x component of the PDV velocity data agrees well with the LDV data. However, there is a difference between the PDV and LDV y component of velocity. There are three possible explanations for this discrepancy. First, the PDV and LDV velocity results were not obtained at exactly the same downstream location. Preliminary three-component PDV results in the same jet flowfield indicate a weak shock structure in the jet, which might influence the y component of velocity.[23] Second, it was assumed that the LDV z-component velocity profile would be the same as the PDV y-component velocity profile, however, the jet is not perfectly axisymmetric. Third, systematic errors involved in the image registration process may also contribute to the discrepancies. The error bars around the x component of velocity is discussed in the error analysis section of the text.

The data shown in Fig. 7 were achieved with subpixel registration accuracy. To demonstrate the significance of image registration accuracy, the data were also processed with the image registration accuracy limited to pixel accuracy and is shown in Fig. 8. As can be seen from Fig. 8, significant errors appear in the x and y components of velocity. The most noticeable errors are seen in the y component of velocity along the horizontal centerline. In comparing Figs. 7 and 8, the errors in the y component of velocity are seen to be significantly reduced using subpixel accuracy, yet the errors are still present. Thus, the remaining errors in the PDV data may stem, at least partially, from systematic errors associated with errors in the pixel registration.

Figure 9 compares the PDV and LDV turbulence intensities along the horizontal centerline. As discussed earlier, image noise, possibly due to speckle, was observed in the raw instantaneous images. The noise did not appear to affect the mean measurements but did affect the turbulence intensities. Some of the effect of the noise was reduced by passing the raw images through a low-pass filter [see Eq. (3)]. The second step to reduce the effect of the noise was to reject points based on a threshold value. The threshold value was set by examining the histogram of the x and y components of velocity

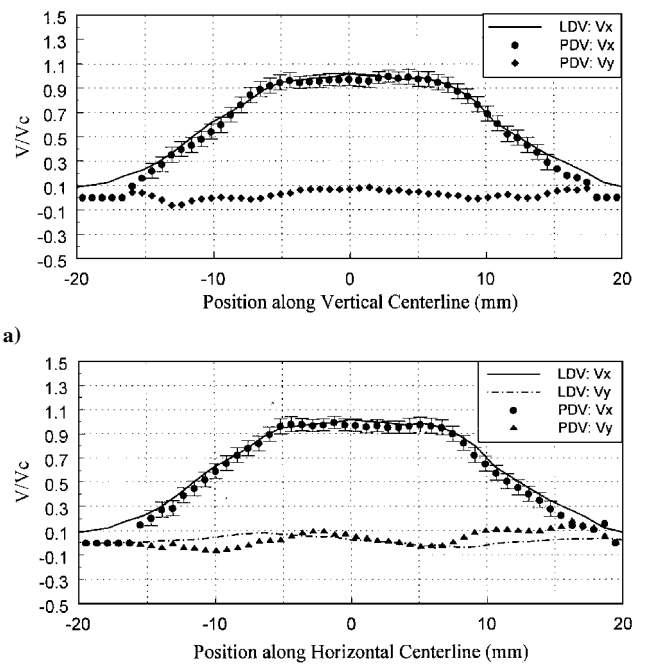

Fig. 7 Comparison of PDV and LDV average velocities with subpixel registration accuracy.

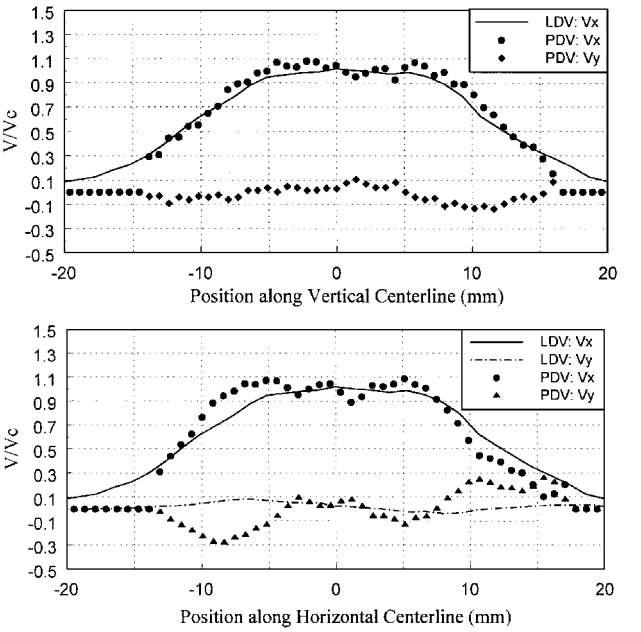

Fig. 8 Comparison of PDV and LDV average velocities with image registration accuracy limited to a pixel.

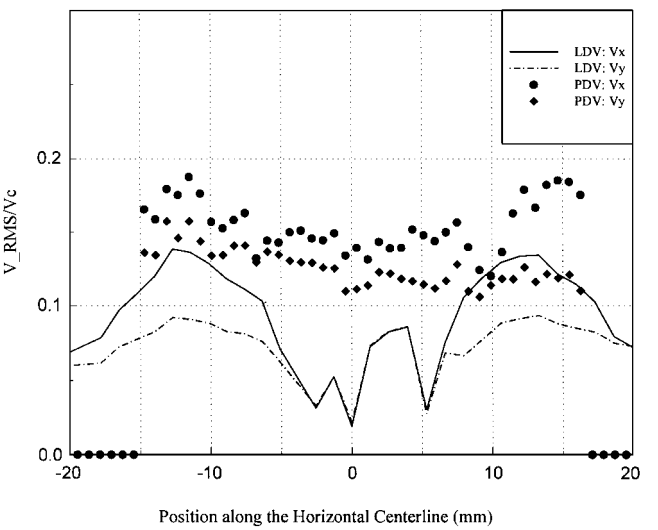

Fig. 9 Comparison of PDV and LDV turbulence intensities along the horizontal centerline; PDV turbulence based on a limited sample size.

for different points in the jet. For the data herein, points where the x component of velocity was greater than 700 m/s or the absolute value of the y component of velocity exceeded 200 m/s were noise dominated and, thus, rejected from the statistical calculations. Note that these are very conservative thresholds because the probability of a velocity falling beyond several standard deviations from the mean in turbulent flow is very small. The shape of the PDV turbulence profile was comparable with the LDV profile. However, the PDV turbulence intensities was notably higher than the LDV values. It was suspected that the small PDV sample size, only 71 images, was a primary factor for the higher turbulence intensities. Preliminary three-component PDV results, with a much larger sample size, indicate turbulence levels of similar magnitude to the LDV data.[23] Residual errors due to the image noise may be another reason for the turbulence intensity discrepancies.

The comparison between the average LDV and PDV results was quite good. The discrepancies between the LDV and PDV y component of velocity may be due to factors concerning the physical characteristics of the flow, as just discussed, and residual registration errors. Furthermore, the turbulence intensities appeared to be converging toward the LDV turbulence intensities. Laser frequency fluctuations and residual image noise might also affect the

turbulence levels. However, because the laser frequency fluctuations are random about a mean, the fluctuations would be primarily averaged out of the mean calculations. Furthermore, because laser drift would shift the profiles in Fig. 7 vertically and because the x component of velocity agrees with the LDV results, laser drift did not seem to be a problem.

V. Uncertainty Analysis

In this section, error sources associated with the PDV technique are discussed and the uncertainty for the present PDV velocity measurements is estimated. Although the sources of error for any PDV experiment will be fundamentally the same, the accuracy of each PDV system will vary because the accuracy is dependent on the details of the PDV system. Furthermore, the sensitivity and accuracy of the PDV experiments are highly dependent on the scalar Doppler equations for the specific PDV system, such as those in Eq. (2), the characteristics of the laser, the details of the filter transmission profile of the filter(s) used, and the dynamic range of the cameras.

Principal sources of error arise from 1) laser frequency variations; 2) image registration: a) Doppler shift calculation and b) velocity component determination; 3) seeder frequency control voltage to laser frequency conversion factor; 4) camera-associated dark charge and readout noise; 5) camera associated photon statistical noise, shot noise, or camera nonlinearity; 6) characterizing the filter transmission profile; 7) filtered and unfiltered image variations: a) camera gain variations, b) split image optical variations, and c) polarization-dependent quality of the beam splitter; 8) angle measurements used in Eq. (2); and 9) image/speckle noise.

The error analysis will proceed in stages. First the error in determining the Doppler shift will be estimated. Then the velocity uncertainty, based on the effect of Doppler shift uncertainty, angle measurement uncertainty, and the registration uncertainty, will be estimated.

Uncertainty in the Doppler Shift Frequency

To minimize systematic errors in the PDV experiment, the procedures and setup used to obtain the filter transmission profile images and the velocity images were virtually identical. The same Doppler shift measuring system and the same laser sheet setup were used when collecting the transmission profile images and the velocity images. In addition, the same normalization procedures, including obtaining and using the flatfield image, and registration procedures were used for both the transmission profiles and velocity measurements.

Errors Associated with Changes in Laser Frequency

In general, the laser frequency and power fluctuate from pulse to pulse and the laser frequency drifts over a long period of time. The rms frequency fluctuation, for the laser used, was measured to be about ± 21 MHz about the mean. This value was used in the uncertainty estimates to be presented. However, it was later found that with optimum seeder alignment the frequency fluctuation could be reduced to ± 10 MHz (Ref. 23). A laser frequency drift is also possible, which is a slow change in frequency over time, that might vary from laser to laser and with room temperature. The frequency fluctuations may affect the turbulence intensities but should be primarily averaged out of the mean velocity calculations. Drift, if present, may affect both. A frequency monitoring system can be used to provide an instantaneous measure of the laser frequency.[12] The laser pulse-to-pulse power fluctuations are normalized out by taking the ratio of the filtered and unfiltered images and was not considered in the error analysis.

Errors Associated with the Molecular Filter

The molecular filter has a filter transmission profile T, which is a function of frequency f. The exact functional relation between T and f is governed by the filter characteristics and may or may not be linear. For example, the work herein used a third-order polynomial to model the filter transmission profile for the instantaneous velocity calculations. However, over smaller frequency ranges, the relationship can be accurately modeled as a linear relationship. To simplify the error analysis, a linear relationship was assumed. The transmission profile was found experimentally by incrementing the seeder frequency control voltage, which increments the laser frequency. A conversion factor from seeder frequency control voltage to laser frequency was required, as discussed earlier. The uncertainty in the determining the frequency of the scattered laser light as a result of the uncertainty in the seeder frequency control voltage to laser frequency conversion factor was estimated to be less than ± 0.5 MHz and was neglected from the overall uncertainty estimates.

To investigate the effect of the error sources on the determination of the Doppler shifted frequency, the filter transmission profile relation can be rewritten as

$$f_e = (T_e/m_c) - (b_c/m_c) \tag{4}$$

where m_c and b_c are the slope and intercept factors characterizing the filter, f_e is the frequency being sought, and T_e is the ratio of the filtered and unfiltered images. The factors b_c and m_c are taken to be steady since the filter temperature remains constant during the entire experiment to within $\pm 1^\circ$C and the filter profiles taken at the beginning and at the end of the experiment for each filter are the same. Errors associated with the filter slope m_c are assumed to be negligible. Thus, with regards to using a molecular filter, the errors stem from uncertainties in the transmission coefficient T_e and the uncertainty in quantifying the filter intercept b_c.

Errors Associated with the Splitter/Recombiner System

The optics of the splitter/recombiner system influence the uncertainty in the transmission coefficient. When using the splitter/recombiner system in conjunction with the filter, the flow image is split, using a beam splitter. One image passes through the filter before being focused on the camera, and the other image is directly focused by the camera. Each image will experience a loss associated with encountering the various optical components in its path. Although a dielectric 50/50 beam splitter is used, the splitting of the light is not exactly 50/50 and is dependent on the polarization of the light. The velocity flatfield image and the transmission profile flatfield image are used to normalize the velocity and transmission profile images, respectively. The flatfield images are taken at the same conditions as the respective data images, except the laser frequency is set to a point corresponding to full filter transmission. This normalization removes polarization and optical variations associated with the splitter/recombiner system. Thus, errors associated with sources 7b and 7c are neglected.

In using the splitter/recombiner system, the accuracy of registering the filtered and unfiltered images is critical in two stages of the PDV data reduction process, in determining the Doppler shift, and in resolving the velocity components. When aligning the filtered and unfiltered images, if the variation in the local signal intensity, $\mathrm{d}I/\mathrm{d}x$, can be approximated, then the pixel intensity error ω_I due to misalignment can be estimated by

$$\omega_I = \Delta x \times \frac{\mathrm{d}I}{\mathrm{d}x} \tag{5}$$

where Δx is the amount of pixel misalignment.[16]

Errors Associated with the Camera

Using the splitter/recombiner system to determine the transmission coefficient, each camera detects a set consisting of a filtered and an unfiltered image. The camera pixel array detects an intensity $I = m\phi + b$, where b is the intensity due to dark charge and readout noise, m is the linearity of the detector and includes the photon statistical noise of the camera, and ϕ is the number of photons incident on the camera. The slope and intercept values may vary from pixel to pixel due to slight array nonuniformities and slightly varying gain values. Errors arise if the slope and intercept values vary with incoming intensity. The variation of the slope is described by the linearity of the camera and is specified as being within $\pm 1\%$ by the camera manufacturer over the range of intensities and gain settings used in the current setup. This nonlinearity includes the inherent shot noise, photon statistical noise, associated with the camera. The nonlinearity of the camera could affect the velocity results and will be included in the analysis. The dark charge and read-out noise portion of the intercept value, however, is reasonably accounted for

by measuring the intensity detected by the camera when the lens cap is in place and by subtracting this value from all of the data and calibration images. Thus, potential residual errors associated with dark charge and readout noise, estimated to be less than ±0.5 MHz, will be neglected. Furthermore, the flatfield images take into account the variation of gain per camera pixel. Thus, the residual errors associated with items 4 and 7a may also be neglected.

Errors Associated with Image Noise

Speckle was the most likely cause of the noise in the instantaneous images. Images obtained from the scattering of coherent light by particles or a surface may be affected by speckle. Speckle is produced when light with sufficient temporal and spatial coherence is scattered by a medium or surface that introduces random optical path fluctuations comparable to the optical wavelength.[21] Other investigators have reported the occurrence of speckle in PDV images.[10,11] The speckle noise to signal ratio was less than 0.15 in the present PDV images. Reference 11 reported a speckle noise to signal ratio range of 0.25–0.30 and Ref. 10 reported ranges of noise to signal level for different configurations starting from 0.40. If the optical path length variation is larger than the wavelength of the light, then the speckle noise to signal ratio is primarily a function of the optics.[24] For this case, the speckle noise to signal ratio can be estimated by knowing the f-number, focal length, and range of the optical system, along with the wavelength of the light and the pixel size.[10,25] Using this approximation, a low estimate of the speckle noise to signal ratio was calculated to be 0.20. This estimate was higher than the noise observed in the current PDV images. Therefore, the speckle in this work was believed to be caused by variations in path length on the order of, if not smaller than the wavelength of the light. The noise did not affect the mean velocity results but did have an impact on the turbulence intensity. The errors associated with the image noise were not modeled in this analysis. However, the two postprocessing steps discussed were used to reduce the effect of the noise.

Resultant Doppler Shift Measurement Error

The method highlighted by Kline and McClintock[26] was used to combine the uncertainty of the remaining sources of error. The combined uncertainty in the frequency was written as

$$\omega_{f_e}^2 = \underbrace{\left[\left(\frac{\partial f_e}{\partial m_f}\times\omega_{m_f}\right)^2 + \left(\frac{\partial f_e}{\partial m_u}\times\omega_{m_u}\right)^2\right]}_{\text{A}} + \underbrace{\left(\frac{\partial f_e}{\partial b_c}\times\omega_{b_c}\right)^2}_{\text{B}} + \underbrace{\left(\frac{\partial f_e}{\partial I}\times\omega_I\right)^2}_{\text{C}} \tag{6}$$

Here ω_i denotes the uncertainty in variable I. The first term, A, represent the uncertainties in the measured frequency f_e due to the 1% nonlinearity of the camera reading. This was taken to arise from the uncertainty in the filtered and unfiltered slopes associated with the camera, m_f and m_u. This includes the photon statistical noise, shot noise, inherent in the detection device. Term A was modeled based on the values that were typical of the data set. For example, the maximum unfiltered signal was approximately 10,000 counts, the filtered image signal ranged from 1400–6000, and the slope of the filter profile was approximated as 0.91 ΔT/GHz. Based on these values, the uncertainty associated with term A was calculated to be ±10 MHz.

Term B represents the uncertainty in the determination of the intercept for the filter transmission profile due to the variation of frequency content of the laser sheet. By properly setting up the laser sheet, as was discussed earlier, most of the variation across the laser sheet can be removed. The laser sheet in the presented system had a 4-MHz variation in frequency. This would imply that the calibrated filter transmission profile intercept value is accurate to ±2 MHz and is effectively term B.

Finally, term C represents the errors in obtaining the transmission coefficient due to errors in image registration. The uncertainty analysis, using Eq. (5), was performed for two regions of the jet, the jet core and the shear layer regions. In the jet core, the intensity was approximately constant; however, due to instantaneous variations, the approximate value of $\mathrm{d}I/\mathrm{d}x = 200$ counts/pixel was used. For the shear layer region, which had a much steeper gradient, the approximate value of $\mathrm{d}I/\mathrm{d}x = 1200$ counts was used. For both the shear layer and the jet core region, the effect of misalignments ranging from 0.1 to 0.5 pixel was investigated by estimating the error on the signal intensity, using Eq. (5), and then, in a manner similar to that of term A, modeling how this affects the Doppler shifted frequency. Although the calculations were preformed for both the jet core and shear layer regions, which are presented in Tables 1 and 2, for clarity most of the discussions will be based on the higher uncertainty associated with the shear layer. The higher uncertainty estimate was ±5 MHz for a 0.1-pixel misalignment and ±22 MHz for a 0.5-pixel misalignment. The accuracy of the pixel registration was expected to be better than 0.5 but not as good as 0.1 pixel. Thus, for the remaining calculations the errors associated with Δx of 0.3 pixel were used.

Table 1 Uncertainty in Doppler shift frequency

Error source	Jet core, ±MHz	Shear layer, ±MHz
Laser frequency fluctuations (no frequency monitoring)	21	21
Laser frequency fluctuations (with potential frequency monitoring)	5	5
Registration of filtered and unfiltered images, $\Delta x = 0.3$	3	14
Registration of filtered and unfiltered images, $\Delta x = 0.1$	1	5
Characterization of transmission profile slope	2	2
Camera nonlinearity including photon statistical noise	10	10
Doppler shift error (no frequency monitoring and $\Delta x = 0.3$)	24	27
Doppler shift error (with potential frequency monitoring and $\Delta x = 0.1$)	11	12

Table 2 Uncertainty in velocity

Error source	Jet core, m/s, $Vx(Vy)$	Shear layer, m/s, $Vx(Vy)$
Angle measurements	7 (6)	7 (6)
Propagation of Doppler shift error (no frequency monitoring and $\Delta x = 0.3$)	24 (16)	28 (18)
Propagation of Doppler shift error (with potential frequency monitoring and $\Delta x = 0.1$)	12 (8)	13 (8)
Pixel misalignment ($\Delta x = 0.3$)	3 (3)	11 (11)
Pixel misalignment ($\Delta x = 0.1$)	1 (1)	4 (4)
Velocity uncertainty (no frequency monitoring and $\Delta x = 0.3$)	25 (17)	31 (22)
Velocity uncertainty (with potential frequency monitoring and $\Delta x = 0.1$)	13 (10)	15 (11)

Summary

Table 1 summarizes the uncertainty in the calculated Doppler shift when using the molecular filter as a frequency discriminator. As was mentioned earlier, the laser frequency fluctuates. The resultant uncertainty in the laser frequency was ±21 MHz, and the combined Doppler shift uncertainty, for the higher uncertainty shear layer region, was ±27 MHz.

This analysis is specifically for the two-component PDV system described earlier. The resultant effect of camera nonlinearity on the velocity results is strongly dependent on the characteristics of

the filter used and the dynamic range of the camera. In addition, the characterization of the transmission profile is dependent on the laser sheet setup. In the preceding analysis, the values represent the typical values seen when using the two-component PDV experiment with relatively strong signal levels of the scattering, 1000–12,000 intensified counts, and with cooled, 14-bit, intensified CCD cameras. References 9 and 10 present a detailed discussion of a more generalized error analysis, designing optimum filters, and the PDV capabilities with various levels of light scattering and camera qualities.

Uncertainty in the Velocity

Errors associated with viewing angle measurements, Doppler shift calculations, and the registration of the images from different DSMSs will propagate into the final velocity calculations.

With regard to the angle measurements, the laser sheet was assumed to be perfectly collimated, based on the negligible change in width with distance of the laser sheet, and the divergence of the collection cone was neglected, due to the large f-number lens used. The error in measuring the viewing direction from the center of the image to the center of the jet core was estimated to be measured within ± 1 deg. The error in velocity, presented in Table 2, was calculated for the x and y components of velocity, for both the jet core and shear layer region. For clarity, however, the text will primarily discuss the larger uncertainty associated with the x-component shear layer region. The error in velocity for V_x due to the angle measurement error was estimated to be ± 7 m/s. This estimation was obtained by determining the difference between the velocities calculated based on the correct angles and the velocities calculated based on angles that were systematically modified by ± 1 deg from the correct angles.

In a similar manner, the effect of the Doppler shift error was determined, for the highest uncertainty case, corresponding to the x-component shear layer region, to be ± 28 m/s.

Accurate registration of the images is extremely important as can be seen from Figs. 7 and 8. The uncertainty in the velocity due to registration errors ω_R associated with aligning images from different DSMSs can be approximated by

$$\omega_R = \lambda \Delta x \times \frac{\mathrm{d}V}{\mathrm{d}x} \tag{7}$$

where V is the Doppler shift Δf_d seen in Eq. (2). The resulting velocity errors are ± 4 m/s for a 0.1-pixel misalignment, ± 11 m/s for a 0.3-pixel misalignment, and ± 17 m/s for a 0.5-pixel misalignment. Image registration accuracy was assumed to be better then 0.3 pixel for the present configuration.

Table 2 summarizes the uncertainty in the velocity measurements associated with each error source. The overall uncertainty in the x component of velocity measurement was ± 25 m/s for the jet core region and ± 31 m/s for the shear layer region. The overall uncertainty for the y component of velocity measurement was ± 17 and ± 22 m/s for the jet core and shear layer regions, respectively. With improved image registration accuracy and utilizing a frequency monitoring system accurate to within ± 5 MHz, the estimated velocity uncertainty can be potentially cut in half.

Although the error analysis was performed for an instantaneous velocity measurement, the PDV and the LDV measurements were not taken simultaneously. As a result, the average PDV velocity profile was compared with the average LDV velocity profile. Furthermore, because the discrepancies between the PDV and LDV measured y component of velocity were partially due to considerations not included in the error analysis, such as the asymmetry of the jet and differences in location of the measurement volume, only the x component of velocity, with the estimated error band, was compared with the LDV measurements. Figure 7 displays the error bar associated with the x component of velocity for the vertical and horizontal centerline. As can be seen, the LDV velocity is within the error band surrounding the PDV velocity.

VI. Concluding Remarks

The PDV technique has been substantially improved. Critical procedural steps were documented and a two-component PDV system was used to make instantaneous measurements of the x and y components of velocity in a two-dimensional plane intersecting the flowfield of a Mach 2, ideally expanded freejet. The PDV velocity measurements compared very well with reference LDV measurements. The error sources inherent in a PDV system were discussed in detail, and an error analysis was performed for the two-component PDV system used herein.

Important procedural steps that were highlighted involved the proper calibration of the splitter/recombiner system, accurate image registration, and careful formation of the laser sheet. The splitter/recombiner system greatly reduces the cost of a PDV setup but must be properly used if accurate velocity measurements are to be obtained. An important step involved with using a splitter/recombiner system was the proper calibration of the system, which should be performed with the filter in place and the laser frequency set to full filter transmission, to obtain flatfield images. Accurately registering the filtered and unfiltered images was another important step in the PDV procedures. Performing the image registration by obtaining a reference image of a grid of white dots on a black background enabled subpixel image registration accuracy. The propagation of errors due to pixel registration errors was demonstrated. Another important step in setting up a PDV experiment was the proper formation of the laser sheet. In general, forming a laser sheet from the centermost portion of the laser beam produced a laser sheet that had a uniform frequency content. The effect of variations in frequency content of the laser beam was demonstrated for two different laser sheet setups.

The results from the two-component PDV system were presented. The planar, instantaneous capabilities of PDV were displayed. The average PDV results were compared with reference LDV results. The x component of velocity compared very well with the LDV data. Discrepancies between the PDV and LDV y-component velocities were discussed and attributed to possible residual image registration errors and physical differences in the PDV and LDV setups. The PDV and LDV turbulence intensities were compared. Although not enough samples were obtained to make a definitive comparison between the PDV and LDV turbulence intensities, it appeared that the PDV turbulence intensities were converging to the LDV turbulence intensities.

A detailed uncertainty analysis was presented, and the overall uncertainty was estimated for the two-component PDV system used in the current research. The overall uncertainty in the x and y components of jet core velocity was estimated to be ± 25 and ± 17 m/s, respectively. The differences between the PDV and LDV reference velocity measurements for the x component of velocity were within the estimated error band. The x component of velocity was within $\pm 5\%$ of the jet centerline velocity. The accuracy of this two-component PDV system was better than or comparable to the accuracy reported by previous investigators using PDV systems in low and high speed flows.

Acknowledgments

The support of this research by the Air Force Office of Scientific Research, with L. Sakell as Technical Monitor, and by the NASA Lewis Research Center, with K. B. Zaman as Technical Monitor, is greatly appreciated.

References

[1] Miles, R. B., Lempert, W. R., and Forkey, J., "Instantaneous Velocity Fields and Background Suppression by Filtered Rayleigh Scattering," AIAA Paper 91-0357, Jan. 1991.

[2] Sabbaghzadeh, J., Buell, W., Holder, J., and Fink, M., "A Very Narrow, High Throughput Rayleigh Filter for Raman Spectroscopy," *Applied Physics B*, Vol. 60, 1995, pp. S261–S265.

[3] Forkey, J. N., Finkelstein, N. D., Lempert, W. R., and Miles, R. B., "Demonstration and Characterization of Filtered Rayleigh Scattering for Planar Velocity Measurements," *AIAA Journal*, Vol. 34, No. 3, 1996, pp. 442–448.

[4] Shirley, J. A., and Winter, M., "Air-Mass Flux Measurement System Using Doppler Shifted-Filtered Rayleigh Scattering," AIAA Paper 93-0513, Jan. 1993.

[5] Elliott, G. S., and Samimy, M., "A Rayleigh Scattering Technique for Simultaneous Measurements of Velocity and Thermodynamic Properties," *AIAA Journal*, Vol. 34, No. 11, 1996, pp. 2346–2352.

[6] Grinstead, J. H., Finkelstein, N. D., Lempert, W. R., and Miles, R. B., "Frequency-Modulated Filtered Rayleigh Scattering: A New Technique for Real-Time Velocimetry," AIAA Paper 96-0302, Jan. 1996.

[7]Elliott, G. S., Samimy, M., and Arnette, S. A., "A Molecular Filter Based Velocimetry Technique for High Speed Flows," *Experiments in Fluids*, Vol. 18, 1994, pp. 107–118.

[8]Arnette, S. A., Samimy, M., and Elliott, G. S., "Two-Component Filtered Planar Velocimetry in the Compressible Turbulent Boundary Layer," AIAA Paper 96-0305, Jan. 1996.

[9]McKenzie, R. L., "Measurement Capabilities of Planar Doppler Velocimetry Using Pulsed Lasers," AIAA Paper 95-0297, Jan. 1995.

[10]McKenzie, R. L., "Planar Doppler Velocimetry Performance in Low-Speed Flows," AIAA Paper 97-0948, Jan. 1997.

[11]Smith, M. W., Northam, G. B., and Drummond, J. P., "Application of Absorption Filter Planar Doppler Velocimetry to Sonic and Supersonic Jets," *AIAA Journal*, Vol. 34, No. 3, 1996, pp. 434–441.

[12]Clancy, P. S., Kim, J.-H., and Samimy, M., "Planar Doppler Velocimetry in High Speed Flows," AIAA Paper 96-1990, June 1996.

[13]Clancy, P. S., and Samimy, M., "Multiple-Component Velocimetry in High Speed Flows Using Planar Doppler Velocimetry," AIAA Paper 97-0497, Jan. 1997.

[14]Komine, H., and Brosnan, S. J., "Instantaneous Three-Component Doppler Global Velocimetry," *Laser Anemometry*, Vol. 1, 1991, pp. 273–277.

[15]Meyers, J. F., Cavone, A. A., and Suzuki, K. E., "Investigation of the Vortical Flow Above an F/A-18 Using Doppler Global Velocimetry," ASME Fifth International Conf. on Laser-Anemometry—Advances and Applications, Aug. 1993.

[16]Thorpe, S. J., Ainsworth, R. W., and Manners, R. J., "Time-Averaged Free-Jet Measurements Using Doppler Global Velocimetry," *Fluids Engineering Division Conference*, Vol. 4, FED-Vol.239, American Society of Mechanical Engineers, New York, 1996, pp. 59–65.

[17]Forkey, J. N., "Development and Demonstration of Filtered Rayleigh Scattering—A Laser Based Flow Diagnostic for Planar Measurement of Velocity, Temperature and Pressure," Final TR, NASA Graduate Student Researcher Fellowship Grant NGT-50826, April 1996.

[18]Yeh, Y., and Cummins, H. Z., "Localized Fluid Flow Measurements with a He-Ne Laser Spectrometer," *Applied Physics Letters*, Vol. 4, 1964, pp.176–178.

[19]Elliott, G. S., Samimy, M., and Arnette, S. A., "A Study of Compressible Mixing Layers Using Filtered Rayleigh Scattering," AIAA Paper 92-0175, Jan. 1992.

[20]Samimy, M., and Lele, S. K., "Motion of Particles with Inertia in a Compressible Shear Layer," *Physics of Fluids A*, Vol. 3, 1991, pp. 1915–1923.

[21]Dainty, J. C., "An Introduction to 'Guassian' Speckle," *Applications of Speckle Phenomena*, edited by W. H. Carter, Vol. 243, Society of Photo-Optical Instrumentation Engineers, Bellingham, WA, 1980, pp. 2–8.

[22]Lim, J. S., and Nawab, H., "Techniques for Speckle Noise Removal," *Applications of Speckle Phenomena*, edited by W. H. Carter, Vol. 243, Society of Photo-Optical Instrumentation Engineers, Bellingham, WA, 1980, pp. 35–44.

[23]Clancy, P. S., Samimy, M., and Erskine, W. R., "Planar Doppler Velocimetry: Three Component Velocimetry in Supersonic Jets," AIAA Paper 98-0506 (to be presented).

[24]Dainty, J. C., "Introduction," *Laser Speckle and Related Phenomena*, edited by J. C. Dainty, Vol. 9, Topics in Applied Physics, 2nd ed., Springer–Verlag, Berlin, 1984, pp. 1–7.

[25]Goodman, J. W., "Statistical Properties of Laser Speckle Patterns," *Laser Speckle and Related Phenomena*, edited by J. C. Dainty, Vol. 9, Topics in Applied Physics, 2nd ed., Springer–Verlag, Berlin, 1984, pp. 9–75.

[26]Kline, S. J., and McClintok, F. A., "Describing Uncertainties in Single Sample Experiments," *Mechanical Engineering*, Jan. 1953, pp. 3–8.

G. Laufer
Associate Editor